

RESEARCH ARTICLE

10.1002/2014JA020123

Key Points:

- Simulations of the current contraction vs. the air pressure
- Transition to the contracted state occurs in hysteresis mode
- BJ formation studied by combination of simulations and existing observations

Correspondence to:

G. M. Milikh,
milikh@astro.umd.edu

Citation:

Milikh, G. M., M. N. Shneider, and M. S. Mokrov (2014), Model of blue jet formation and propagation in the nonuniform atmosphere, *J. Geophys. Res. Space Physics*, 119, 5821–5829, doi:10.1002/2014JA020123.

Received 23 APR 2014

Accepted 18 JUN 2014

Accepted article online 24 JUN 2014

Published online 16 JUL 2014

Model of blue jet formation and propagation in the nonuniform atmosphere

G. M. Milikh¹, M. N. Shneider², and M. S. Mokrov³

¹Department of Astronomy, University of Maryland, College Park, USA, ²Department of Mechanical and Aerospace Engineering, Princeton University, USA, ³Institute of Problems in Mechanics, RAS, Moscow, Russia

Abstract About two decades ago, researchers discovered upward propagating flashes of light originating above thunderstorms. Due to their distinctive, principally blue color, they were named “blue jets” (BJ). The broadly accepted production mechanism of a BJ is through a lightning leader which rises through the nonuniform atmosphere. Specifically, the formation of the initial lightning leader is thought to be governed by the contraction of the current of a streamer flash into a small radius channel. This paper presents results of simulations of the current contraction in the air as a function of both the pressure and convective heat removal time. We have shown that transitions to the contracted state occur in a hysteresis mode that allows both contracted and diffusive states to coexist. We have obtained the critical current for this phase transition and studied the formation and propagation of BJs in the atmosphere through a combination of quantitative models and existing observations of BJs that combine optical images with the data of the electric current carried by the jets.

1. Introduction

Luminous flashes above thunderstorms have been reported by eyewitnesses for over a century and eventually documented from low-light optical observations on the ground [Franz *et al.*, 1990; Gerken and Inan, 2005]. However, only during the Sprites94 aircraft campaign Wescott *et al.* [1995] identified the class of upward propagating stratospheric flashes, named blue jets (BJ) due to its primarily blue color. Brief upward jets, which propagate only a few kilometers and terminate below 25 km, were dubbed blue starters (BS) [Wescott *et al.*, 1996]. Pasko *et al.* [2002] discovered the so-called gigantic blue jets (GBJ), propagating into the lower ionosphere. Then, GBJ events have been detected from the ground [Su *et al.*, 2003] and identified from the imager ISUAL onboard Formosat-2 [Kuo *et al.*, 2009]. Recent observations were able to detect simultaneous optical images and low-frequency magnetic fields [Cummer *et al.*, 2009; Lu *et al.*, 2011; Chou *et al.*, 2011]. In fact, Lu *et al.* [2011] observed that “the gigantic jet-producing flash began as ordinary intracloud lightning with upper level channels attempting to exit the cloud, and then produced the upward gigantic jet. The leader progression of one event was detected at altitude above 20 km.”

Earlier theoretical models suggested that BJ are similar to the streamer zone of a leader (streamer corona) [Petrov and Petrova, 1999]. Krehbiel *et al.* [2008] conjectured “that blue jets occur as a result of electrical breakdown between the upper storm charge and the screening charge attracted to the cloud top.” It was following the occurrence of negative cloud-to-ground (–CG) flash that changes the electric field in the cloud. GBJs originated from the midlevel charge layer and propagate upward. Rioussat *et al.* [2010] developed a model that accounts for the time-dependent conduction currents and screening charges formed due to the thundercloud charge sources. Raizer *et al.* [2007, 2010] developed a model of bipolar BJ assuming that the opposite-polarity leaders grow in opposite directions and supply each other with the charge via the highly conductive channel. Evidently, if the bi-leader is initiated in the anvil, one of the leaders can extend beyond the cloud top.

Gallimberti [1979] was the first who noted that the development of atmospheric lightning is initiated and sustained by the formation of streamer corona and leader discharges in air, very similar to those observed in laboratory long sparks. A critical issue, which is still unresolved, is the conversion from the streamer to leader phase.

Popov [2003] and Bazelyan *et al.* [2007] presented models based on the hypothesis that the formation and development of a leader are governed by the contraction of the current of a streamer flash into a small radius channel which heats gas to the critical temperature of an arc discharge. Gas pressure increases rapidly near

the axis of the plasma channel, and subsequent dynamic processes decrease the gas density, which increases E/N (reduced electric field, with N = neutral gas density) and the increased E/N feeds back into a sharp increase in the ionization rate. Newly ionized electrons are heated, transfer their energy to the gas via electron-neutral collisions, which excite vibration modes of the gas, which then undergo V-T relaxation. This gives rise to the thermal-ionization instability, constituting a universal mechanism to perturb homogeneous discharges at sufficient pressure and high electric currents in atomic and molecular gases. The instability can cause discharge contraction: formation of current filaments with higher temperature and ionization than ordinary glow discharges. Since the thermal-ionization instability develops from transverse inhomogeneities while the electric field remains homogeneous along the current direction, a comprehensive model of it should be at least two dimensional.

However, a number of simplified 1D models of current contraction in different gases were developed [Jaeger *et al.*, 1976; da Silva and Pasko, 2013]. Some models of current contraction based on the development of volume instabilities also took into account the large scale of inhomogeneities of the electric field due to the electrodes design and the nonuniform density and composition of the gas [Akishev *et al.*, 1993; Korolev and Mesyats, 1991]. Chemical reactions could also play a role [da Silva and Pasko, 2013]. The existing theoretical models are limited to a formation of an individual streamer [Bazelyan and Raizer, 2000; Ebert *et al.*, 2010; Li *et al.*, 2009; Pancheshnyi *et al.*, 2005]. A few attempts were made to describe formation of a leader by semi-empirical 1D models [Bazelyan *et al.*, 2007; Arevalo and Cooray, 2011; da Silva and Pasko, 2013].

Recently, we developed a self-consistent, 2D model of current contraction with axisymmetric geometry that was able to describe the current contraction in pure molecular nitrogen [Shneider *et al.*, 2012]. Later, it was generalized to simulate the current contraction in air [Shneider *et al.*, 2013], where it includes considerations of electron attachment to molecular oxygen, collisional electron detachment, and convective heat removal that closely resembles horizontal wind in the atmosphere.

This paper presents results of simulations of the current contraction in the air above a thunderstorm as a function of both the pressure, and of convective heat removal time. We have shown that transitions to the contracted state occur in a hysteresis mode that allows both contracted and diffusive states to coexist. We have obtained both the critical current for this phase transition and studied the formation and propagation of BJ's in the atmosphere through a combination of quantitative models and experimental observations of the critical contraction current.

2. The Model Description and Results of Simulations

The whole set of equations is given in Appendix A along with the boundary conditions. Here we present general description of the model. The model is naturally divided into three coupled blocks. The first block deals with the plasma: it solves the continuity equations for electrons (equation (A1)) positive (equation (A2)) and negative ions (equation (A3)) along with the charge conservation equation (equation (A4)). The output of this block is the electron density, temperature, and the current characteristics. The second block derives the gas heating source. It computes the pumping rates of vibrational and electronic levels of gas molecules (equation (A5)) and then describes the energy transfer to the gas kinetic temperature due to the V-T relaxation (equation (A6)). The third block solves gas dynamics equations for the neutral gas density and temperature (equation (A7)). Under constant pressure the increase in the gas temperature leads to the gas expansion, reducing the number density, and thus increasing the reduced electric field E/N . That in turn increases the ionization and molecular excitation rates by the free electrons.

Dynamics of the current contraction strongly depends on the type of the molecular gas used. In fact, nitrogen shows well-pronounced growth of the contracted channel, while in the air under relatively high pressure the contraction develops simultaneously in the whole volume. It is related to the different mechanisms responsible for the charge sink. In fact, under the high air pressure the main role is played by the electron attachment to O_2 in the three-body collisions, while at the low pressure the main role is played by the electron-ion recombination and convective removal of the charges, like that occurs in the nitrogen.

The plates in Figure 1 show the spatial distribution of the normalized electron density formed at 0.5, 0.6, and 0.8 ms from an assumed initial perturbation of the gas temperature. The 2D model of a plane gap discharge in air under 50 Torr pressure and ambient temperature $T_0 = 293$ K, the ambient electron density $n_0 = 10^{12} \text{ cm}^{-3}$

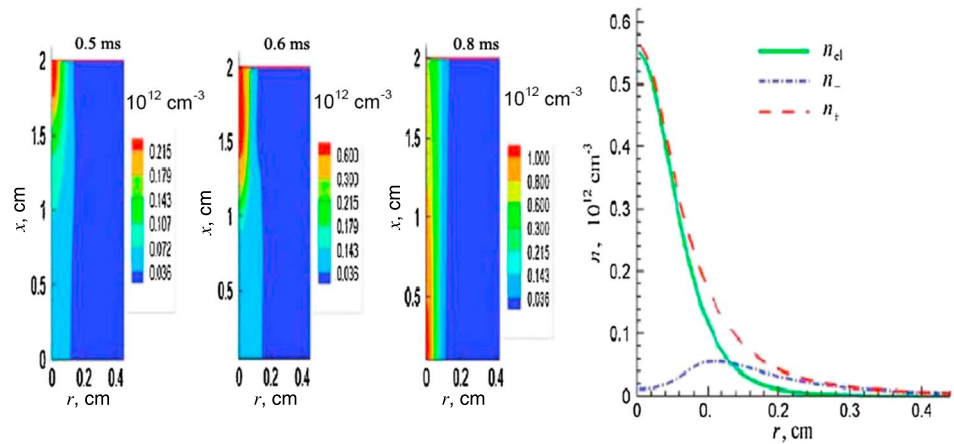


Figure 1. (a, b, c) Simulations of the temporal evolution of 2D electron density; (d) the radial distribution of the densities of electrons, positive, and negative ions occurs at $t = 8 \times 10^{-4} \text{ s}$.

is used. The electromotive force of 9 kV is applied to the electrodes, the external ohmic resistance is 500 kOhms, and the space between electrodes is 2 cm. Due to space symmetry of the model, we adopt a computational box which is only half size of the physical domain. The computational region lies on one side of the symmetry axis of the channel contraction. It is shown that the plasma filament was formed and expanded in both x and y directions. At the same time, the vibrational temperature of N_2 and O_2 , and the gas temperature of air increase [Shneider *et al.*, 2012]. It reveals that the current comes to the final contracted distribution in $\sim 1 \text{ ms}$.

During the dynamic contraction the profiles of electron density $n_e(r)$, gas temperature $T(r)$, and vibrational temperature $T_v(r)$ in the various sections of the channel become increasingly steep with time, and the area occupied by the current narrows [Shneider *et al.*, 2013]. This process is inhomogeneous along the x ; in areas closer to the initial perturbation, the contracted state forms faster. The radial plasma distribution at 0.8 ms is illustrated by Figure 1d.

3. Hysteresis

Our model shows that transition to the contracted state in air occurs in hysteresis mode, in which, the two stable states exist simultaneously; it is also often called “hard mode” [Shneider *et al.*, 2012]. It is shown by Figure 2 (the top panel) where the contracted regimes are shown by the red trace, while the homogeneous regimes are shown by the blue trace. The simulations were made for 78% of N_2 and 22% of O_2 at 100, 50, and 10 Torr. The diffuse (on the bottom) and contracted regime (on the top) are marked by the arrows. The critical current I_{cr} is shown by the downward arrow; if $I < I_{cr}$ the discharge is uniform, and at $I > I_{cr}$ the contracted channel is formed. The bottom plot in Figure 2 reveals I_{cr} as a function of the air pressure.

The critical current for the transition from the diffuse to contracted state depends on the gas pressure. It increases when the pressure (density) of the background gas reduces as shown in Figure 2. It is due to the fact that reduction of the air pressure increases the rate of the ambipolar diffusion while the gas heating due to the V-T relaxation becomes weaker; thus, the efficiency of the current contraction drops with the falling pressure.

4. Discussion

We discuss formation and propagation of BJs in the atmosphere through a combination of simulations of the critical contraction current and selected direct observations which will be used for the calibration purposes. Let us assume that the current carried by the leader that forms the bright stem of BJ is constant. The leader consists of the contracted hard core surrounded by diffusive halo, such as in the discussed above model. When the leader moves up in the atmosphere the critical current required for the phase transition (i.e., contraction) increases. The leader reaches its termination height z_{term} when the current it carries becomes smaller than the local critical contraction current ($I \leq I_{cr}(z_{term})$).

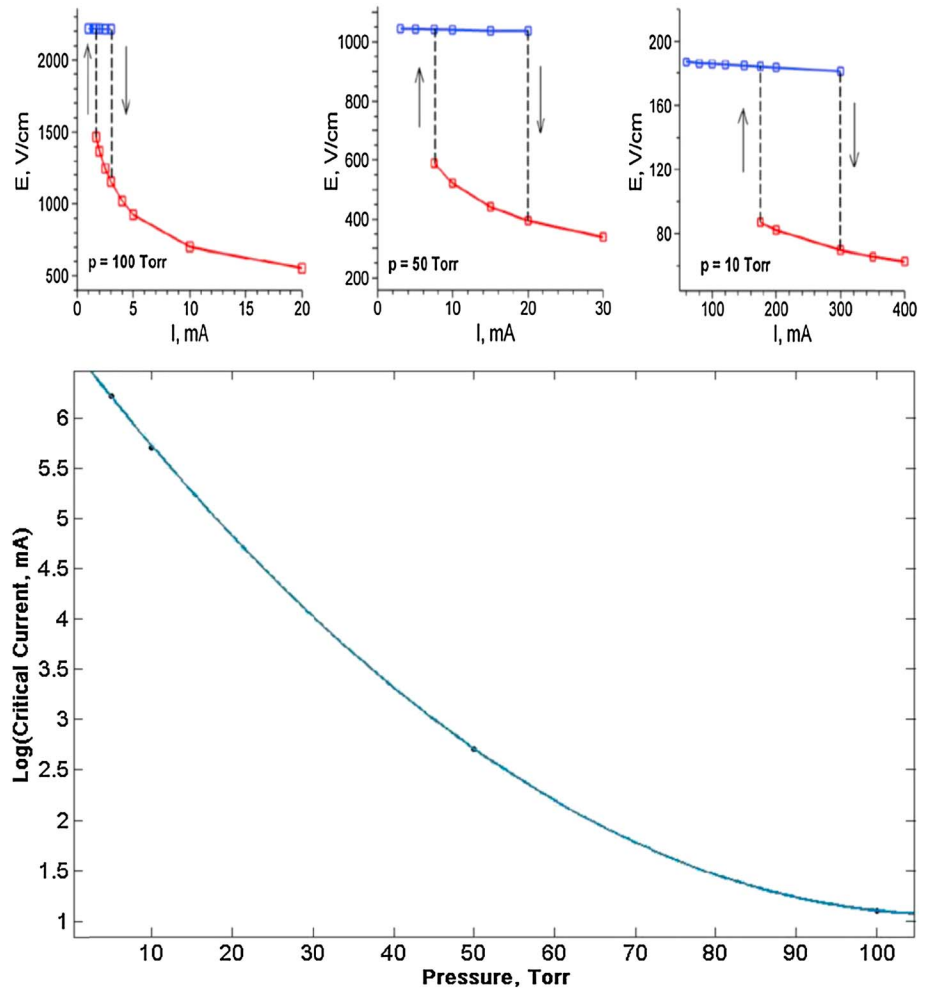


Figure 2. The top row shows the current-voltage characteristic of the glow discharge in the air flow at different pressures. The (bottom) diffuse and (top) contracted regime are marked by the arrows. The critical current I_{cr} is marked by the downward arrow; if $I < I_{cr}$ the discharge is uniform, and if $I > I_{cr}$ the contracted channel is formed. The bottom plot reveals I_{cr} as a function of the air pressure.

The dependence of the critical current I_{cr} upon air pressure from Figure 2(bottom) is converted into the dependence of I_{cr} upon the altitude by using MSIS E-90 atmosphere model (see Figure 3). Furthermore, we analyze the existing observations of BJ's choosing those that combine optical images with the data of the electric current carried by the jets. The latter were obtained from the low-frequency magnetic field measurements. We chose the two multi-instrumental observations, *van der Velde et al.* [2010] and *Lu et al.* [2011].

From the BJ image we define the top edge of the bright stem that we conjecture as the termination height of the leader. The insert on Figure 3 reveals the image of BJ [*van der Velde et al.*, 2010]; here the top edge of the bright stem is located at 48 km.

We assume that at 48 km the 3.3 kA current carried by the BJ becomes insufficient to support transformation from the diffusion to the contracted phase. Thus, at the leader termination height 48 km $I_{cr} = 3.3$ kA.

The main inaccuracy of the BJ measurements is related to the large distance error because the precise BJ position is unknown but most likely associated with the colder convective cloud tops, as was assumed by all GBJ work to date. From the analysis by *van der Velde et al.* [2010] it is known that in the observed GBJ the error in the height detection ranges between -7% and 3% . Thus, the top of the bright stem is located at 48 ± 2.5 km, while in the *Lu et al.* [2011] experiment it was at 28 ± 2.5 km, (provided by Steven Cummer) with

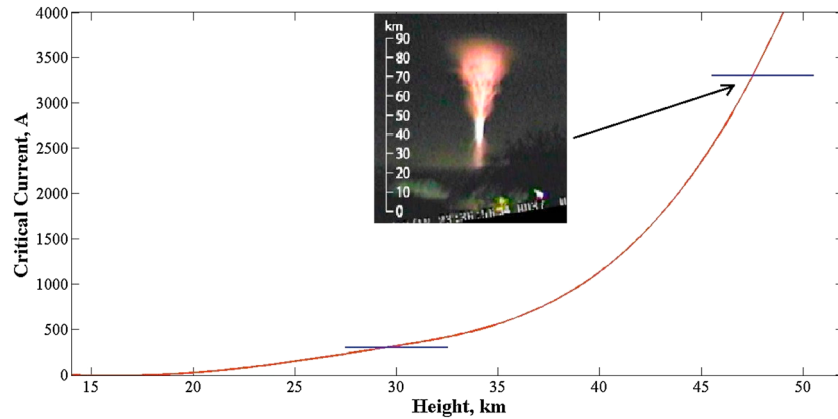


Figure 3. The critical current in the atmosphere vs. altitude. Two horizontal bars centered at 28 and 48 km obtained from the observations by *Van der Velde et al.* [2010] and *Lu et al.* [2011], respectively. The insert shows the image of GBJ obtained by *van der Velde*.

the jet current at 300 A. Furthermore, the critical current in Figure 3 was calibrated in such a way that its value at the mean termination height of the leader at 28 and 48 km coincides with the current observed during the two quoted BJ events.

The contraction model includes convective heat removal time (τ) in the continuity equations for the electron density and the air temperature (see Appendix A). It is similar to the effect of the horizontal wind in the atmosphere. Therefore, we apply a cylindrical model of BJ with the radius r to find the wind velocity $v_w \approx 2r/\tau$ which $\tau = 1$ ms and $r = 2$ cm, used in our simulations, gives $v_w = 40$ m/s. Figure 4a reveals comparison of the two current-voltage characteristics of the glow discharge obtained under different convective heat removal time (squares correspond to 1 ms, triangles correspond to 5 ms). Figure 4b shows simulations of the critical current vs. convective heat removal time at 20 and 50 Torr, which correspond to 25 and 20 km, respectively. The BJ critical current vs. velocity of the horizontal wind for 20 and 25 km is presented on Figure 4c. It was computed using results of Figure 4a and the normalization factor from Figure 3.

Another possible mechanism of BJ termination is short-circuiting by the streamers that escape to the ionosphere. As mentioned by *Neubert et al.* [2011] when the GBJ "reaches a certain altitude, propagating as a leader, its streamers may jump all the way to the ionosphere." Earlier *Raizer et al.* [2007] found that streamer can escape to the ionosphere from the height h_{esc} if the following condition is fulfilled

$$h_{esc} = \Delta \times \log\left(\frac{E_{s0}\Delta}{U_L}\right) \tag{1}$$

where $\Delta = 7.2$ km is the atmospheric scale height, U_L is the electric field potential at the leader tip, and E_{s0} is the critical field required for the streamer growth at standard conditions for the temperature and pressure. In fact, for positive streamers $E_{s0} = 326$ kV/m [*Raizer et al.*, 2010]. Assuming that the potential is caused by the cloud-to-ground discharge, which transferred the charge Q_0 , the potential at the escape height is

$$U_L = \frac{Q_0}{4\pi\epsilon_0(h_{esc} - h_0)} \tag{2}$$

where h_0 is the altitude of the charge reservoir and ϵ_0 is the permittivity of free space. By substituting equation (2) into equation (1) we get

$$h_{esc} = \Delta \times \log\left(4\pi\epsilon_0 \frac{E_{s0}\Delta}{Q_0} [h_{esc} - h_0]\right) \tag{3}$$

From the analysis by *Neubert et al.* [2011] of the observations of the GBJ by *van der Velde et al.* [2010] it was found that the current moment has three distinct pulses, and we will focus on the second positive polarity pulse. The estimates show that it was generated by the charge $Q_0 = 35$ C centered at $h_0 = 6$ km. Equation (3) was solved numerically using the above values of Q_0 and h_0 . It was found that $h_{esc} \approx 42$ km,

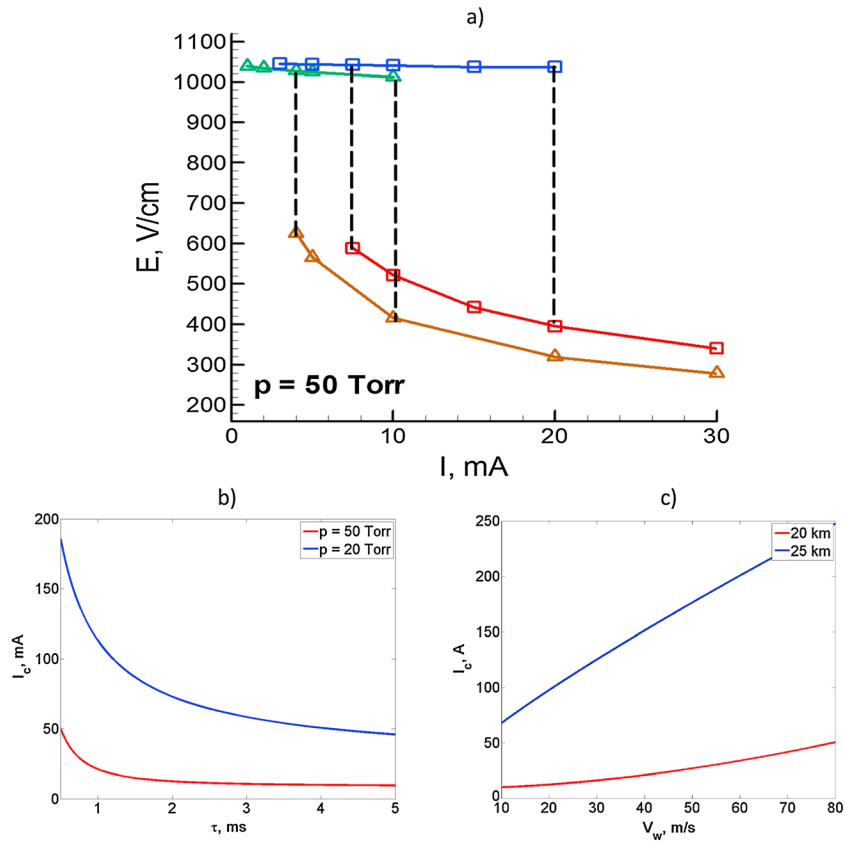


Figure 4. Comparison of the two current-voltage characteristics of the glow discharge obtained under different convective heat removal time (squares correspond to 1 ms; triangles correspond to 5ms) (a). Simulations of the critical current vs. convective heat removal time at 20 and 50 Torr (b). The BJ critical current vs. velocity of the horizontal wind for 20 and 25 km (c).

which is consistent with the observations. Note the BJ stops at the height where U_L drops below the ionization threshold of the air, which occurs at a moderate charge value Q_0 . Detailed description of this mechanism is out of scope of this paper.

The above analysis allows us to estimate the difference between starters, blue jets, and gigantic blue jets based on the amount of current they carry. As shown above, in the nonuniform atmosphere, the stoppage height of

a leader is determined by the critical current for the transition from the diffuse to contracted state, i.e., by the current the leader carries. Figure 5 is slightly modified Figure 3 where the current carried by a blue jet is shown vs. the stoppage height. The latter is presented by the top of the bright stem observed in the discussed above experiments. Furthermore, it is widely accepted that the stoppage height for a starter is about 25 km which corresponds to the current $I < 100$ A carried by the leader (see Figure 5). Fully developed blue jets have the stoppage height between 25 and 40 km, which corresponds to $110 \text{ A} < I < 1000 \text{ A}$ carried by the leader. Finally, when the leader goes above 40 km, its streamers fly to the ionosphere making a gigantic blue jet. It requires the current I been in access of 1000 A.

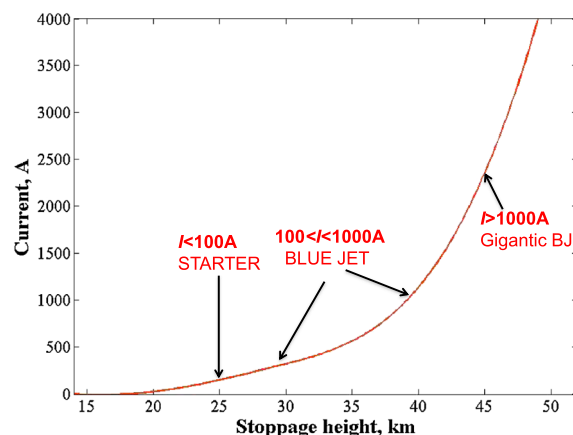


Figure 5. The current carried by a blue jet as a function of the stoppage height.

5. Conclusions

In conclusion, a self-consistent model of the current contraction in air has been developed. This model allows a hysteresis regime of contraction. The critical current for the transition from the diffuse to contracted state depends on the air pressure and on the convective heat removal time. We assume that at the leader termination height the current inside BJ is not sufficient to support transformation from the diffusion to the contracted phase.

The study of BJ formation based on the combination of the model simulations and existing BJ multi-instrumental observations was conducted. It allows us to find the critical current in the atmosphere as a function of altitude. Such analysis helps us to estimate the difference between starters, blue jets, and gigantic blue jets based on the amount of current they carry.

The transversal wind plays an important role in the BJ development. In fact, the critical current of the fully developed BJ ranges between 60 and 240 A if the horizontal wind velocity changes from low 8 m/s to severe 80 m/s.

Estimates made on the charge transferred by the CG discharge causative of the GBJ, which allows the streamers to escape to the ionosphere, show agreement with the GBJ observations [van der Velde et al., 2010].

Finally, it is worth to mention that blue jets can be modeled in laboratory as in the case of red sprites [Opaits et al., 2010]. Such experiments could lead to a better understanding of the mechanisms of BJ formation.

Appendix A: Mathematical Description of Current Contraction in Air

We consider the current contraction in the positive column. The respective set of equations consists of continuity equations for the densities of electrons, n_e , positive n_+ , and negative n_- ions, equation for the electric field \mathbf{E} , gas translational, T , and vibrational, T_v , temperatures, and equation for the electric circuit. The continuity equations for n_e , n_+ , and n_- are:

$$\frac{\partial n_e}{\partial t} + \nabla \cdot \Gamma_e = Q_e, \quad (A1)$$

$$\frac{\partial n_+}{\partial t} + \nabla \cdot \Gamma_+ = Q_+, \quad (A2)$$

$$\frac{\partial n_-}{\partial t} + \nabla \cdot \Gamma_- = Q_-, \quad (A3)$$

where $\Gamma_e = -n_e \mu_e \mathbf{E} - D_e \nabla n_e$, $\Gamma_+ = n_+ \mu_+ \mathbf{E}$, and $\Gamma_- = -n_- \mu_- \mathbf{E}$ are the corresponding fluxes of charged particles; μ_e , μ_+ , and μ_- are their mobilities; D_e is the electron diffusion coefficient; and τ is the characteristic time for convective removal of charged particles (and heat) from the discharge. Source terms in the right-hand sides of (A1)–(A3) are $Q_e = (v_{ion} - v_a)n_e + v_d n_- - \beta_{e+} n_e n_+ - \frac{n_e}{\tau}$, $Q_- = v_a n_e - v_d n_- - \beta_{ii} n_- n_+ - \frac{n_-}{\tau}$, and $Q_+ = Q_e + Q_-$.

Here v_{ion} , v_a , and v_d are the ionization, attachment, and detachment frequencies; β_{e+} and β_{ii} are the coefficients for electron-ion and ion-ion recombination; in the plane geometry, $\tau \approx L_z/u$ is the characteristic time of convective plasma cooling with laminar gas flow parallel to the electrodes (L_z is the characteristic scale length along the flow), and u is the flow velocity. In the assumed cylindrical geometry $\tau \approx 2r_{max}/u$, where r_{max} is the radius of the domain occupied by the weakly ionized plasma. The discharge model is treated by assuming quasi-neutrality of the plasma positive column. If the quasi-neutrality condition $n_+ = n_e + n_-$ is fulfilled one of the equations (A1)–(A3) becomes redundant. Therefore, we have solved equations (A1) and (A3) for n_e and n_- , while n_+ was obtained as a sum of n_e and n_- in each point.

The electric field $\mathbf{E} = -\nabla\phi$ is determined from the charge conservation equation

$$\nabla \cdot \mathbf{j} = 0, \quad \mathbf{j} = -e(\Gamma_e - \Gamma_+ + \Gamma_-). \quad (A4)$$

A significant fraction of the power released in a discharge in air is pumped to the vibrational degrees of freedom. However, in view of rapid V-T relaxation of oxygen molecules, we assumed that in the air the

vibrational energy is stored in the nitrogen molecules. Thus, the balance equation for the vibrational energy E_V yields:

$$\frac{\partial E_V}{\partial t} - \frac{\partial}{\partial x} \left(D \frac{\partial E_V}{\partial x} \right) - \frac{1}{r} \frac{\partial}{\partial r} \left(r \left(D \frac{\partial E_V}{\partial r} \right) \right) = \eta_V j_e E - \hbar \omega \Pi - \frac{E_V - E_V^0}{\tau_{VT}} - \frac{(N_0/N) [E_V - E_V^0(T_0)]}{\tau} \quad (A5)$$

Here D is the diffusion coefficient for N_2 molecules, $E_V = x_{N_2} N \hbar \omega_{N_2} / (\exp(\hbar \omega_{N_2} / k T_V) - 1)$, $\hbar \omega_{N_2} = 0.292$ eV is the vibrational quanta of N_2 molecules; E_V^0 is the equilibrium value of E_V ; Π is the flow of vibrational quanta in the vibrational energy domain, which describes the energy sink that brings the upper vibrational levels down; η_V is the fraction of Joule heat responsible for the vibrational excitation; τ_{VT} is the VT relaxation time of the vibrational levels; $x_{N_2} = 0.8$ is the N_2 fraction, $T_0 = 293$ K, $N_0 = p / (k T_0)$, and p is the gas pressure. The functions Π and η_V are taken from Raizer *et al.* [1995].

As the pressure is equalized quickly, we can assume that the gas is heated under isobaric conditions. In this case the gas density N and temperature T are related as $N \propto T^{-1}$. For T we get the equation:

$$N c_{p1} \frac{\partial T}{\partial t} - \frac{\partial}{\partial x} \left(\lambda(T) \frac{\partial T}{\partial x} \right) - \frac{1}{r} \frac{\partial}{\partial r} \left(r \left(\lambda(T) \frac{\partial T}{\partial r} \right) \right) = \eta_T j_e E + \hbar \omega \Pi + \frac{E_V - E_V^0}{\tau_{VT}} - N_0 c_{p1} \frac{T - T_0}{\tau} \quad (A6)$$

Here c_{p1} is the specific heat of air at a constant pressure; $\lambda(T)$ is the molecular heat conductivity; and $\eta_T = 1 - \eta_V$ is the fraction of Joule heat responsible for the direct heating of the gas.

The calculations were performed for the electron and ion mobility adopted from [Raizer, 1991]: the ionization rate by electron impact, the rate of collisional detachment, and the electron attachment rate in the three-body collisions were taken from Kossyi *et al.* [1992] and Macheret *et al.* [2001, 2002].

Similar to the model of contraction in nitrogen [Shneider *et al.*, 2012] we assume that

$$p = N k T = \text{const}, \quad (A7)$$

where k is the Boltzmann constant.

We used the following boundary conditions for the equation set (A1), (A3)–(A6): since the near-electrode region is excluded from consideration, we assume that $\partial n_e / \partial x = \partial n_- / \partial x = \partial T / \partial x = \partial E_V / \partial x = 0$ on the electrodes boundaries (at $x = 0$, $x = L_x$). For the electric potential we have $\varphi = 0$ at $x = 0$ and $\varphi = V$ at $x = L_x$, where V is the discharge voltage. It is assumed that $\partial n_e / \partial r = \partial n_- / \partial r = \partial T / \partial r = \partial E_V / \partial r = \partial \varphi / \partial r = 0$ on the symmetry axis ($r = 0$) and on the side wall of the discharge chamber ($r = r_{\text{max}}$).

Acknowledgments

The data for this paper are available at: <http://spp.astro.umd.edu/SpaceWebProj/Projects%20n%20research%20pages/High%20Alt%20Light.htm>. We would like to thank Dr. Steve Cummer for providing us results of his observations. GM appreciates helpful discussions with Chris Najmi. The work is supported by the NSF Aeronomy Program.

Michael Balikhin thanks Jan Blecki and an anonymous reviewer for their assistance in evaluating this paper.

References

- Akshes, Y. S., A. A. Deryugin, V. B. Karal'nik, I. V. Kochetov, A. P. Napartovich, and N. I. Trushkin (1993), Numerical simulation and experimental study of an Atmospheric-Pressure Direct-Current Glow Discharge, *Plasma Phys. Rep.*, *20*(6), 511–524.
- Arevalo, L., and V. Cooray (2011), Preliminary study on the modeling of negative leader discharges, *J. Phys. D Appl. Phys.*, *44*, 315204, doi:10.1088/0022-3727/44/31/315204.
- Bazelyan, E. M., and Y. P. Raizer (2000), *Lightning Physics and Lightning Protection*, IOP, Bristol, U. K., and Philadelphia, Pa.
- Bazelyan, E. M., Y. P. Raizer, and N. L. Aleksandrov (2007), The effect of reduced air density on streamer-to-leader transition and on properties of long positive leader, *J. Phys. D Appl. Phys.*, *40*, 4134–4144, doi:10.1088/0022-3727/40/14/007.
- Chou, J. K., L. Y. Tsai, C. L. Kuo, Y. J. Lee, C. M. Chen, A. B. Chen, H. T. Su, R. R. Hsu, P. L. Chang, and L. C. Lee (2011), Optical emissions and behaviors of the blue starters, blue jets, and gigantic jets observed in the Taiwan transient luminous event ground campaign, *J. Geophys. Res.*, *116*, A07301, doi:10.1029/2010JA016162.
- Cummer, S. A., J. Li, F. Han, G. Lu, N. Jaugey, W. A. Lyons, and T. E. Nelson (2009), Quantification of the troposphere-to-ionosphere charge transfer in a gigantic jet, *Nat. Geosci.*, *2*, 617–620, doi:10.1038/NGEO607.
- da Silva, C. L., and V. P. Pasko (2013), Dynamics of streamer-to-leader transition at reduced air densities and its implications for propagation to lightning leaders and gigantic jets, *J. Geophys. Res. Atmos.*, *118*, 13,561–13,590, doi:10.1002/2013JD020618.
- Ebert, U., S. Nijdam, C. Li, A. Luque, T. Briels, and E. van Veldhuizen (2010), Review of recent results on streamer discharges and and discussion of their relevance for sprites and lightning, *J. Geophys. Res.*, *115*, A00E43, doi:10.1029/2009JA014867.
- Franz, R. C., R. J. Nemzek, and J. R. Winckler (1990), Television image of a large upward electrical discharge above a thunderstorm, *Science*, *249*, 48.
- Gallimberti, I. (1979), The mechanism of long spark formation, *J. Phys.*, *40*, 193–198.
- Gerken, E. A., and U. S. Inan (2005), Streamers and diffuse glow observed in upper atmospheric electrical discharges, *IEEE Trans. Plasma Sci.*, *33*(2), 282–283.
- Jaeger, E. F., L. Oster, and A. V. Phelps (1976), Growth of thermal constrictions in a weakly ionized-gas discharge in helium, *Phys. Fluids*, *19*(6), 819.
- Korolev, Y. D., and G. A. Mesyats (1991), *The Physics of a Pulsed Breakdown of Gases*, Nauka, Moscow, Russia.
- Kossyi, I. A., A. Y. Kostinsky, A. A. Matveyev, and V. P. Silakov (1992), Kinetic scheme of the non-equilibrium discharge in nitrogen-oxygen mixtures, *Plasma Sources Sci. Technol.*, *1*, 207–220.
- Krehbiel, P. R., J. A. Riousset, V. P. Pasko, R. J. Thomas, W. R. Wison, M. A. Stanley, and H. E. Edens (2008), Upward electrical discharges from thunderstorms, *Nat. Geosci.*, *1*, 233–237, doi:10.1038/ngeo162.

- Kuo, C. L., et al. (2009), Discharge process, electric fields, and electron energy in ISUAL-recorded gigantic jets, *J. Geophys. Res.*, *114*, A04314, doi:10.1029/2008JA013791.
- Li, C., U. Ebert, and W. Hundsdorfer (2009), 3D hybrid computations for streamer discharges and production of runaway electrons, *J. Phys. D Appl. Phys.*, *42*, 202,003.
- Lu, G., et al. (2011), Lightning development associated with two negative gigantic jets, *Geophys. Res. Lett.*, *38*, L12801, doi:10.1029/2011GL047662.
- Macheret, S. O., M. N. Shneider, R. B. Miles, and R. J. Lipinski (2001), Electron-beam-generate plasmas in hypersonic magnetohydrodynamic channels, *AIAA J.*, *39*, 1127–1138.
- Macheret, S. O., M. N. Shneider, and R. B. Miles (2002), Modeling of air plasma generation by repetitive high-voltage nanosecond pulses, *IEEE Trans. Plasma Sci.*, *30*, 1301–1314.
- Neubert, T., O. Chanrion, E. Arnone, F. Zanotti, S. Cummer, J. Li, M. Füllekrug, S. Soula, and O. van der Velde (2011), The properties of a gigantic jet reflected in a simultaneous sprite: Observations interpreted by a mode, *J. Geophys. Res.*, *116*, A12329, doi:10.1029/2011JA016928.
- Opaits, D. F., M. N. Shneider, P. J. Howard, R. B. Miles, and G. M. Milikh (2010), Study of streamers in gradient density air: Table top modeling of red sprites, *Geophys. Res. Lett.*, *37*, L14801, doi:10.1029/2010GL043996.
- Pancheshnyi, S. V., M. Nudnova, and A. Y. Starikovskii (2005), Development of a cathode directed streamer discharge in air at different pressures: Experiment and comparison with direct numerical simulation, *Phys. Rev. E*, *71*, 016407, doi:10.1103/PhysRevE.71.016407.
- Pasko, V. P., M. A. Stanley, J. D. Mathews, U. S. Inan, and T. G. Woods (2002), Electrical discharge from a thundercloud top to the lower ionosphere, *Nature*, *416*, 152–154.
- Petrov, N. I., and G. N. Petrova (1999), Physical mechanisms for the development of lightning discharges between a thundercloud and the ionosphere, *Tech. Phys.*, *44*, 472–475.
- Popov, N. A. (2003), Formation and development of a leader channel in air, *Plasma Phys. Rep.*, *29*(8), 695–708.
- Raizer, Y. P. (1991), *Gas Discharge Physics*, Springer, Berlin, Germany.
- Raizer, Y. P., M. N. Shneider, and N. A. Yatsenko (1995), *Radio-Frequency Capacitive Discharges*, CRC, Boca Raton, Fla.
- Raizer, Y. P., G. M. Milikh, and M. N. Shneider (2007), Leader–streamer nature of blue jets, *J. Atmos. Sol. Terr. Phys.*, *69*, 925–938, doi:10.1016/j.jastp.2007.02.007.
- Raizer, Y. P., G. M. Milikh, and M. N. Shneider (2010), Streamer- and leader-like processes in the upper atmosphere: Models of red sprites and blue jets, *J. Geophys. Res.*, *115*, A00E42, doi:10.1029/2009JA014645.
- Riousset, J. A., V. P. Pasko, P. R. Krenbiel, W. Rison, and M. A. Stanley (2010), Modeling of thundercloud screening charges: Implications for blue and gigantic jets, *J. Geophys. Res.*, *115*, A00E10, doi:10.1029/2009JA014286.
- Shneider, M. N., M. S. Mokrov, and G. M. Milikh (2012), Dynamic contraction of the positive column of a self-sustained glow discharge in molecular gas, *Phys. Plasmas*, *19*(3), 033512, doi:10.1063/1.3694913.
- Shneider, M. N., M. S. Mokrov, and G. M. Milikh (2013), Dynamic contraction of the positive column of a self-sustained glow discharge in nitrogen/air flow, 51st AIAA Aerospace Sciences Meeting, Grapevine, Dallas/Ft. Worth Region, Tex., 7–10 Jan., doi:10.2514/6.2013-1186.
- Su, H. T., R. R. Hsu, A. B. Chen, Y. C. Wang, W. S. Hsiao, W. C. Lai, L. C. Lee, M. Sato, and H. Fukunishi (2003), Gigantic jets between a thundercloud and the ionosphere, *Nature*, *423*, 974–976.
- van der Velde, O. A., J. Bor, J. Li, S. A. Cummer, E. Arnone, F. Zanotti, M. Füllekrug, C. Haldoupis, S. NaitAmor, and T. Farges (2010), Multi-instrumental observations of a positive gigantic jet produced by a winter thunderstorm in Europe, *J. Geophys. Res.*, *115*, D24301, doi:10.1029/2010JD014442.
- Wescott, E. M., D. Sentman, D. Osborne, D. Hampton, and M. Heavner (1995), Preliminary results from the Sprites94 aircraft campaign, 2, Blue jets, *Geophys. Res. Lett.*, *22*, 1209–1212, doi:10.1029/95GL00582.
- Wescott, E. M., D. D. Sentman, M. J. Heavner, D. L. Hampton, D. L. Osborne, and O. H. Vaughan Jr. (1996), Blue starters: Brief upward discharges from an intense Arkansas thunderstorm, *Geophys. Res. Lett.*, *23*, 2153–2156, doi:10.1029/96GL01969.